J. Am. Soc. Mass Spectrom. (2019) 30:1654–1662
DOI: 10.1007/s13361-019-02276-6

RESEARCH ARTICLE

Topological Characterization of Coordination-Driven Self-assembly Complexes: Applications of Ion Mobility-Mass Spectrometry

Christopher S. Mallis,[1] Manik Lal Saha,[2] Peter J. Stang,[2] David H. Russell[1]

[1]Department of Chemistry, Texas A&M University, College Station, TX 77843, USA
[2]Department of Chemistry, University of Utah, Salt Lake City, UT 84112, USA

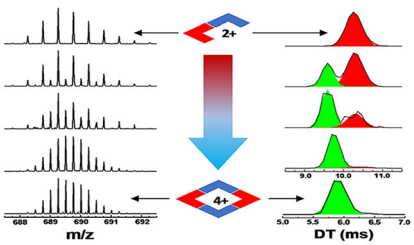

Abstract. Coordination-driven self-assembly (CDSA) is increasingly used to synthesize coordination complexes containing metal-centered electron acceptors and typically nitrogen-containing electron donors. Characterization of the structures obtained from CDSA via crystallographic or spectroscopic means is limited due to difficulties in forming single crystals for X-ray studies and overlapping precursor and product signals in NMR. Here, we employ ion mobility-mass spectrometry (IM-MS), which provides a direct measure of size and shape of the CDSA complexes, to study the intact reaction products of a rhomboid-shaped complex. This approach negates the need for product isolation and crystallization and allows for tracking of the product distribution as a function of time. A potential challenge of IM-MS is that the size/shape of the observed CDSA complexes can vary with internal energy; however, we show that proper tuning of the instrument reduces the effects of collisional activation thereby allowing for retention of ion conformations that reflect solution-phase ion structures.

Keywords: Ion mobility-mass spectrometry, Coordination-driven self-assembly, Supramolecular coordination complex

Received: 17 December 2018/Revised: 30 May 2019/Accepted: 21 June 2019/Published Online: 17 July 2019

Introduction

Self-assembly (SA) allows the spontaneous formation of ordered systems at all scales from the organization of weather systems to the formation of molecular crystals [1]. A subclass of SA reactions includes coordination-driven self-assembly (CDSA) reactions which form highly selective complexes through the coordination of nitrogen-containing donor ligands and metal-containing acceptor ligands [2]. Pioneering work from Lehn [3–5], Stang [6–9], Fujita [10–12], Wesdemiotis [13–15], and others has driven the design, synthesis, and characterization of a variety of CDSA reaction products. CDSA reaction products have been designed for use as catalysts, chemical sensors, drug transporters, and theranostic agents with recent success [7, 9, 16–20]. However, their characterization is complicated by overlapping signals of precursor and product signals in NMR spectroscopic measurements, and CDSA products can be difficult to crystallize due to intrinsic physicochemical properties, such as void space. Additionally, their weak coordinating bonding networks are intrinsically dynamic in structure, and thus greatly benefit from characterization techniques that can measure condensed-phase structures or conformers [1].

Mass spectrometry (MS) and ion mobility-mass spectrometry (IM-MS) have been used to characterize intact supramolecular ions with the measured masses and gas-phase conformers related back to solution chemistry and crystal structures [21–23]. The high mass resolution afforded by modern mass spectrometers provides accurate determination of elemental composition from nominal masses and correlation of

Electronic supplementary material The online version of this article (https://doi.org/10.1007/s13361-019-02276-6) contains supplementary material, which is available to authorized users.

Correspondence to: David Russell; *e-mail:* russell@chem.tamu.edu

complex isotopic distributions to the identity and number of metal centers in organometallic ions [24]. Specifically, IM provides an orthogonal separation of gas-phase ions based on their size-to-charge ratio and allows for determination of ion-neutral collision cross sections (CCS) from which conformational or structural information can be interpreted [25, 26]. Drift tube–based IM instruments separate ions based on size-to-charge ratio as they are transported by an electrostatic field filled with a buffer gas (typically helium or nitrogen). The traveling wave-based IM instrumentation uses a set of stacked ring ion guides to superimpose a traveling wave over the radiofrequency ion guide, wherein small ions travel with the wave and larger ions roll over the wave. Additionally, IM can separate isobaric ions which have overlapping *m/z* signals, yet different elemental compositions. Due to the high rotational symmetry of many CDSA product ions, the gas-phase dissociation of intact complexes will often produce isobaric ions as both the mass and charge of the ions are reduced by the same factor.

Wesdemiotis and coworkers used traveling wave IM-MS to separate and identify isobaric reaction and dissociative product ions of several metallated terpyridine macrocyclic complexes and have identified cyclic and linear gas-phase conformers [13–15]. Brocker *et al.* demonstrated that supramolecular square, triangle, and triangular prism structures can be characterized by IM-MS with their CCS agreeing well-reported crystal structures; however, their mass spectra contain a host of identified fragment ions [27]. While these results are promising, the reported MS shows a host of fragments and multiple charge states, and there is limited discussion on the effects of improper instrument tuning on the observed IM-MS spectra.

While IM-MS has demonstrated ability to observe gas-phase conformers of a range of biomolecular ions (e.g., peptides, proteins, protein complexes), recent literature suggests that the sampling conditions (i.e., instrument tune settings) can greatly affect the sampled conformation space [28–31]. Here, we show that by properly tuning an IM-MS instrument, intact ions having low internal energies and minimal anion binding can be observed by IM-MS in high relative abundances. Additionally, collision-induced dissociation (CID) of the observed intact product ions reveals the topology of the rhomboid products and suggests that anionic adducts provide for Coulombic stabilization of self-assembly products in the gas phase.

Methods

Sample Preparation

The Pt-based precursor **1** and pyridine-based precursor **2** (1,3-bis(pyridin-4-ylethynyl)benzene) were dissolved separately in HPLC-grade acetone (EMD Chemicals, NJ, USA) and mixed to a final product concentration of ~ 50 μM prior to being loaded into borosilicate capillary tips (~ 20-μm O.D.). A platinum wire was placed in contact with the solution inside the glass capillary to facilitate electrospray.

Ion Mobility-Mass Spectrometry

The Waters Synapt G2 (Manchester, UK) was operated in the positive mode as a nESI-Q-TWIMS-TOF and has been described in detail elsewhere [32]. Briefly, after nanoelectrospray ionization (nESI), the ions generated can be mass selected in the quadrupole (Q), collisionally activated in the trap region prior to mobility separation, separated in the traveling wave ion mobility (TWIM) cell, and finally analyzed with a time-of-flight (TOF) mass analyzer. The IMS operates with three regions: trap, IMS, and transfer with a helium cell located between the trap and IMS regions. For pre-IMS CID experiments, ions are mass selected in the Q and collisionally activated in the trap region. Capillary voltages were set to ~ 1.3 kV. For instrument tuning and CID experiments, traveling wave height was set to 10 V, wave velocity was set to 200 m/s, and IM nitrogen flow rate was set to 50 mL/min. Additional parameter values are included in the Supplemental Information.

Following instrument tuning methods similar to those published on ubiquitin and metallothionein for reducing the effective temperature of ions [28], a tuning grid was developed to study the effects of instrument tuning on the observed MS (Figure S1). Select MS spectra are shown in Figure 2. Additionally, observed fragmentation pathways for the rhomboid and nitrate-adducted rhomboid ions are shown in Scheme 2 to label the identified ions. After tuning optimization, CID experiments were performed on the nitrate-free (**3**) and nitrate-adducted (**7**) rhomboid ions by mass selecting them in the quadrupole and increasing the collision voltage (CV) in the trap region up to a maximum of 40 V. The MS results of these CID experiments are presented in Figure S5.

Due to the non-uniform electric field applied along the mobility device, external calibrant ions are required to convert an experimental traveling wave-based ATD to a rotationally averaged CCS. While CCS calibrants have been developed for proteins and polymers [33–35], none have been developed for the ions studied herein. Therefore, IM ATDs were not converted to CCSs.

Data Processing and Relative Abundance Determination

IM-MS data were processed using MassLynx 4.1 (Waters Corporation, Manchester, UK). Gaussian peak fitting of select IM spectra was performed using Origin 8 (OriginLab Corporation, Northampton, MA). Theoretical MS isotope distributions were calculated with ChemCalc [36]. Comparisons of experimental and theoretical isotopic distributions are included in the Supplemental Information (Figure S6).

Determination of relative ion abundances was performed using the IM data rather than the MS data. Relative IM abundances (RA_{IM}) were calculated as the ratio of the Gaussian peak fit area of identified ions to the total integrated area of the IM spectra. For example, an RA_{IM} of 50% would indicate that half of the total ion signal is found under the Gaussian fit of an identified ion. These steps are necessary due to the overlapping signals in the mass spectra of the full (**3**) and half-rhomboid (**4**)

ions. In this way, the relative abundances of isobaric ions can be quantified for the processing of CID data. A visual explanation of the RA_{IM} determination is provided in the Supplementary Material (Figure S2).

Results

Supramolecular Rhomboid Product Ions

The combination of the 60° bite angle between the square planar Pt(II) acceptors of precursor **1** and the 120° difference between the pyridine donor ligands of precursor **2** (see Scheme 1) yields the CDSA of a molecular ion with a rhomboidal supramolecular shape and an overall charge of 4+ (ion **3**, *m/z* 689) from loss of four nitrate anions (two from each precursor **1**). Lower charge ions are formed from adduction of counterions in solution, as is observed with the nitrate-adducted rhomboid ion, with an overall charge of 3+ (ion **7**, *m/z* 940). For clarity, ions resulting from gas-phase dissociation or fragmentation are identified in Scheme 2.

Reduction of Ion Internal Energies

To observe intact, solution-phase ion structures in the gas phase by IM-MS, the internal energy of the ions must remain below their respective dissociation thresholds. Default instrument tuning parameters promote high transmission of ions; however, these instrument conditions result in ions identified as products of dissociation and fragmentation of intact ions formed in solution. The ion with the highest relative abundance under these default conditions is identified as the nitrate-free analogue to the bis-Pt(II) precursor ion, **5** (*m/z* 549) (Figure 1A). Effects of in-source activation and dissociation are mitigated by reduction of source potentials including the source and extraction cones (Figure 1B) where the relative abundance of the nitrate-free rhomboid **3** as well as the half-rhomboid **4** is observed in higher relative abundance. Finally, progressive tuning was completed by reduction of the trap bias potentials, increasing the flow to the pre-IM helium cell, and reducing the nitrogen flow to the IM cell (Figure 1C). The finalized instrument parameters were selected to promote transmission of the intact nitrate-free and nitrate-adducted rhomboid ions (**3** and **7**, respectively) as the most abundant ions. A larger grid of instrument tuning parameters is available in the Supporting Information (Figure S1).

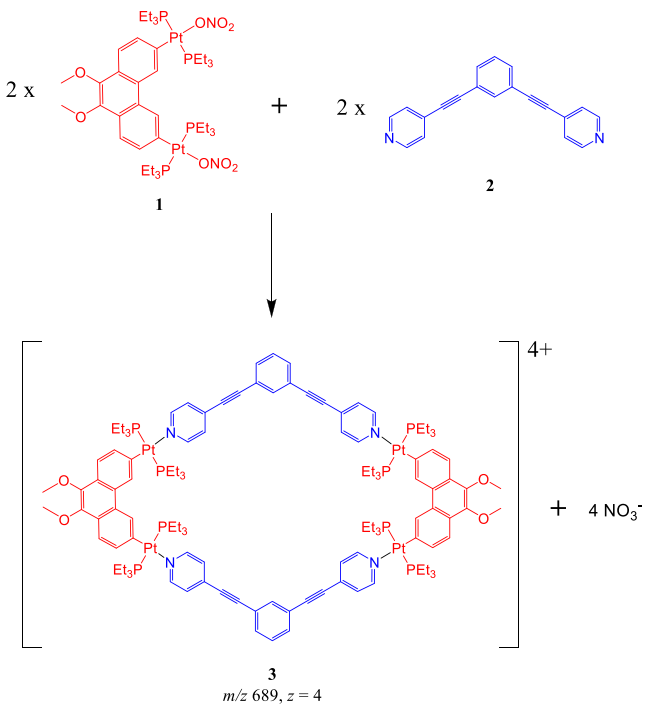

Scheme 1. Solution mixing of precursors **1** and **2** in acetone solutions at room temperature results in the formation of the charged rhomboid ion **3** with four nitrate counterions

One of the problems with mass spectral characterization of many coordination-driven self-assembly products is the high degree of rotational symmetry of the reaction products. As a result, collisional activation of intact ions can lead to loss of mass and charge such that the *m/z* values of the precursor and product ions are the same. IM is implemented as an orthogonal separation tool for these isobaric ions, where the conformational heterogeneity of all ions can be observed, and the relative abundances of isobaric ions can be determined.

Secondary tuning of the IM separation conditions was performed by changing the traveling wave height and wave velocity while maintaining constant drift times of the rhomboid ion, **3** (*m/z* 689) (Supplemental Figure S3). Others have noted that increasing wave height leads to narrowing of IM peak widths and increasing wave velocity leads to widening of mobility peak widths [37]. To maintain constant ion drift times, both the wave heights and velocities must increase (or decrease). As a result, the observed changes in peak widths are minimal as relative increase and decrease in peak widths effectively cancel each other.

Collision-Induced Dissociation of Intact Complexes

Collision-induced dissociation (CID) of the observed rhomboid complexes (nitrate-free rhomboid, **3**, and nitrate-adducted rhomboid, **7**) was performed to confirm topology of the reaction products. CID was accomplished through mass selection of the precursor ions of interest, collisional activation in the pre-IM trap region with increasing collision voltages (CV), separation in the TWIMS cell, then mass analysis of observed dissociative or fragmentation products in the TOF. Relative abundances of the identified products were determined using the previously described methods and are shown in Figure 2A, B and dissociation pathways are presented in Scheme 2. Example mass spectra for low and moderate collision voltages are presented in Figure 2C, D for the nitrate-free rhomboid **3** and nitrate-adducted rhomboid **7**, respectively.

CID of the nitrate-free rhomboid **3** reveals three sequential dissociation steps (Figure 2A). First, the intact rhomboid **3** dissociates to the isobaric half-rhomboid **4** with a maximum relative abundance observed at a CV of 10 V. Next, the half-

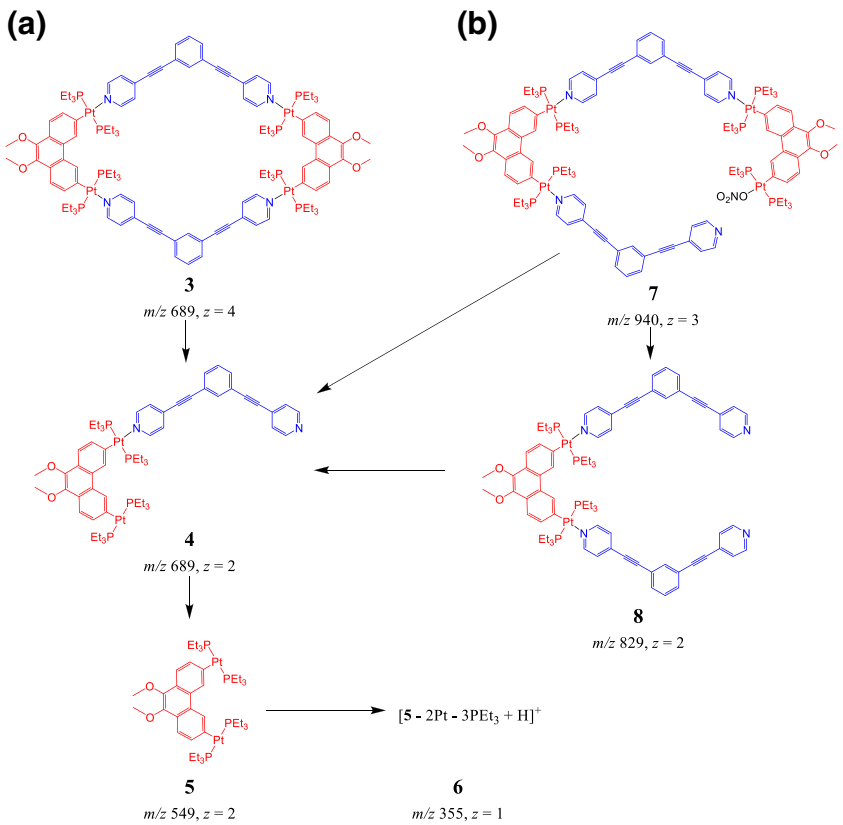

Scheme 2. General structures, *m/z*, and charge state (*z*) of ions identified in the mass spectra resulting from CID of (**a**) the nitrate-free rhomboid **3** and (**b**) the nitrate-adducted rhomboid **7**

rhomboid **4** loses its bis-pyridine ligand **2** to form the denitrated Pt-precursor ion **5** with a maximum relative abundance observed at 20 V. The final step involves fragmentation of the Pt-precursor ion **5** to form ion **6** with an undetermined structure, but with a mass and isotope pattern corresponding to [**5** – 2 Pt – 3 PEt_3 + H]$^+$.

CID of the nitrate-adducted rhomboid **7** reveals four sequential dissociation steps (Figure 2B). The first two dissociative products are observed at 15 CV. These two products are identified: **8** is formed from the loss of [**5** + NO_3^-]$^+$ and the half-rhomboid **4** is formed from the loss of a nitrate-adducted half-rhomboid ion. The half-rhomboid **4** can also result from the loss of one of its bis-pyridine ligand **2** from the observed ion **8**. Continued dissociation and fragmentation of the half-rhomboid ion **4** then follows a similar pattern as observed with the half-rhomboid **4** from the dissociation of the nitrate-free rhomboid **3**, wherein ion **4** loses its bis-pyridine ligand **2** to form a nitrate-free precursor ion **5** before fragmenting to ion **3**.

Survival Yield Comparisons

From the plots of the relative abundance of the CID precursor ions (either **3** or **7**) as a function of collision voltage (Figure 2), it is apparent that the nitrate-adducted rhomboid **7** survives until significantly higher collision voltage compared with the nitrate-free rhomboid **3**. Converting collision voltages to laboratory-frame collision energies (E_{lab}) can normalize for the relative collision energies of different charge states at the same collision voltages, since at the same collision voltage, an ion with higher charge will experience a greater acceleration (larger collision forces) into the collision cell than an ion with lower charge. Even when normalizing for effects of different ion charges in the collision cell, it is still apparent that the nitrate-free rhomboid **3** ions are more fragile than the nitrate-adducted rhomboid **7** ions. This result is likely due to the greater destabilizing Coulombic repulsion of ions with higher charge, wherein the charge reduction associated with nitrate adduction results in more stable gas-phase ions.

The survival yield (SY) abundances of the CID precursor ions were then plotted as a function of E_{lab} of the CID precursor ions (Figure 3) to normalize for collision energy as ions with higher charge will experience greater acceleration in the collision cell. After fitting the SY data to sigmoidal curves, the inflection points were used to determine CE_{50} values for each precursor ion where half of the initial relative abundance is observed. Fitting of these data reveals CE_{50} values of 32.0 eV for the nitrate-free rhomboid **3** ion and 40.4 eV for the nitrate-adducted rhomboid **7** ion. While this manipulation is used as an attempt to mitigate the effects of different charge states when exposed to similar collision potentials, the difference in these energies is likely a result

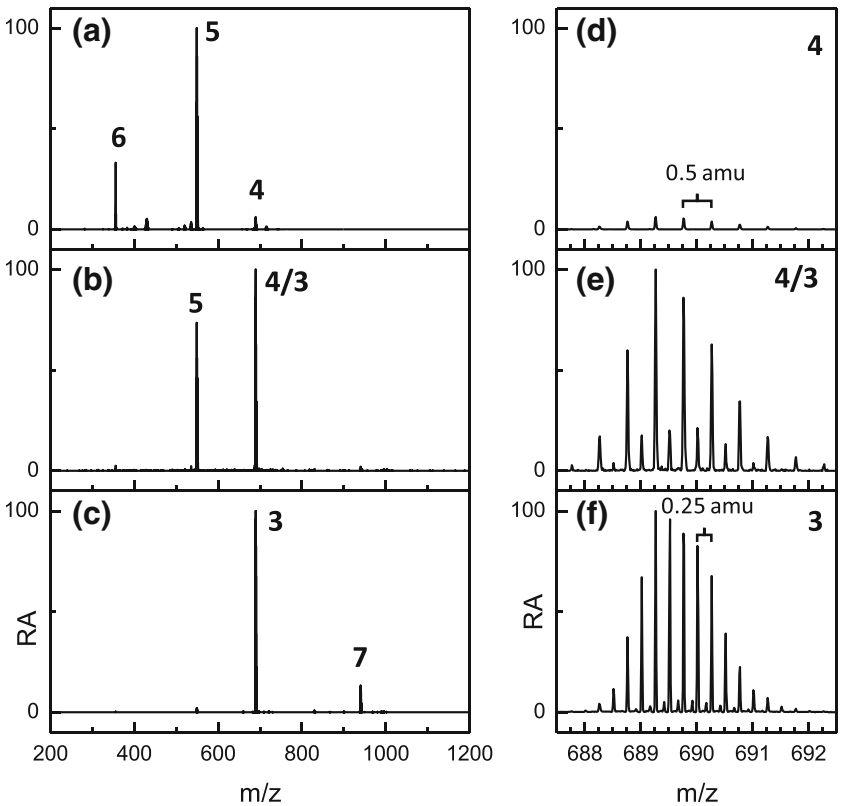

Figure 1. The effects of instrument tuning on the observed mass spectra are revealed. (**a**) Dissociation products dominate the mass spectrum under default tuning conditions. (**b**) Reduction of the source and extraction cone potentials reveals some intact rhomboid **4** in low relative abundance. (**c**) Reduction of the trap bias voltage, increasing the helium cell flow, and decreasing the IM nitrogen flow rates show the rhomboid ions **3** and **7** with the largest relative abundances. (**d**–**f**) Expansion of the mass spectrum around *m/z* 690 of **a**–**c**, respectively, reveals the isobaric mass spectrum of the half-rhomboid ions (**4**, $z = 2$) and intact rhomboid ions (**3**, $z = 4$) with isotopic spacings of 0.5 and 0.25 amu, respectively

of increased Coulombic repulsion effects, wherein the ion with more charge sites may be driven to dissociate at lower energies. Overall, these data suggest an increase in gas-phase stability with the addition of the nitrate anion.

Discussion

The utility of IM-MS as a reaction product characterization technique is dependent on its ability to preserve intact, solution-phase reaction products through separation and detection in the gas phase. Through proper tuning of the TWIMS-MS instrument, we show that intact, high-charge complexes can be ionized and transmitted through the instrument in high relative abundances. For the first time, counterion-free CDSA reaction product ions are observed from the mixture of precursors without prior isolation of reaction product complexes. Observed CDSA ion charge states are dependent primarily on the number of metal centers and anion adducts, such that reduction in observed nitrate adducts leads to increase in ion charge and consequently an increase in repulsive Coulombic forces. Therefore, high-charge complexes require careful instrument tuning to observe intact ions with internal energies below their respective dissociation thresholds.

The specific utility of IM herein is two-fold. First, IM is used as a separation tool for the isobaric nitrate-free full rhomboid **3** and the half-rhomboid **4** ions. These ions are separated using IM such that their relative abundances can be determined from the observed mobility spectra. Second, the IM distribution of each identified ion can be fit to single Gaussian peaks with high coefficients of determination ($R^2 > 0.995$ for all fits). Therefore, all identified ions adopt singular conformers in the gas phase, or other conformers are indistinguishable at the given IM resolution. Unlike what has been observed with triangular CDSA complexes having a similar coordination motif [27], multiple conformers (i.e., open and closed) of these rhomboidal ions were not observed at either charge state.

After tuning, mass selection and collisional activation (i.e., CID) of the observed nitrate-free and nitrate-adducted rhomboid ions (**3** and **7**, respectively) confirm the topologies of the ions. The sequential losses observed and highlighted in Scheme 2 and Figure 2 show that the dissociation pathways of the two rhomboid ions to the half-rhomboid ion **4** are different. The nitrate-free rhomboid **3** dissociates in half to form the half-rhomboid at relatively low collision energies, while the nitrate-adducted rhomboid **7** appears to lose its nitrate adduct in its first dissociative loss either as a nitrate-adducted analogue of the fragment **5** (i.e., $[\mathbf{5} + NO_3]^+$) to form **8** or a nitrate-adducted

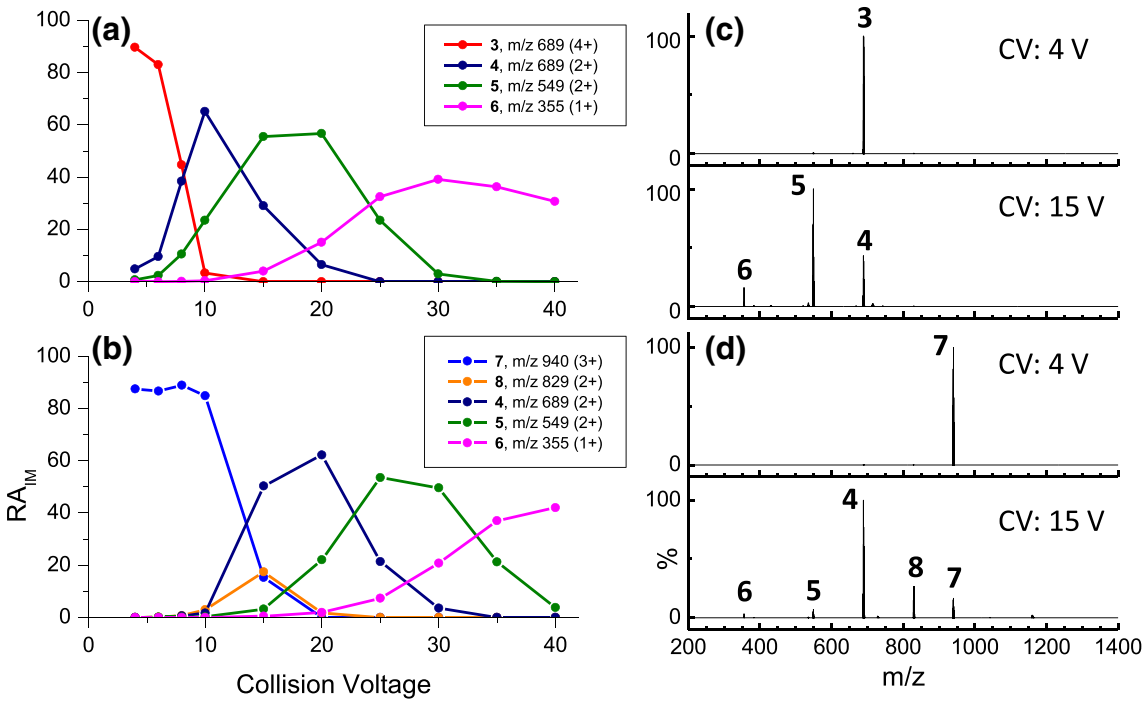

Figure 2. Plot of the relative IM abundances (RA_{IM}) as a function of trap collision voltage for the CID of (**a**) the nitrate-free rhomboid ion **3** and (**b**) the nitrate-adducted rhomboid **7**. (**c**, **d**) Example MS spectra resulting from the CID of **3** and **7**

analogue of the half-rhomboid ion **4** (i.e., $[\mathbf{4} + NO_3]^+$) to form **4**. Because the appearance energies of these two observed dissociative products are the same (15 V), it appears that these ions are both formed from the nitrate-adducted rhomboid **9** at lower collision energies and at higher collision energies, the half-rhomboid ion **4** may be formed from the loss of one bis-pyridine ligand **2** from ion **8**. Additionally, the IM drift times do not change as a function of collision voltage, and each ion can be fit to single Gaussian distributions throughout the CID experiment (see Figure 4); therefore, ions are observed to dissociate rather than rearrange or unfold in the gas phase.

Overall, these dissociation results suggest that the nitrate adduct is coordinated to one of the Pt centers of the rhomboid complex and may disrupt closure of the rhomboid ring. Without experimentally determined CCS and crystallographic structures of these ions, these conjectures cannot be definitively confirmed. Calibration of CCS on the traveling wave-based IM separations requires calibrants with similar interaction potentials to the buffer gas and the ions studied herein and which have not been previously established. While other calibrant systems are available, they have been primarily designed and tested for CCS determination of peptide [38] and protein ions [33, 39].

With proper CCS calibrants and MD simulations of candidate structures, it may be possible to determine the overall structure of the nitrate-adducted rhomboid, although the CCS difference between open and closed rhomboid conformers may be minimal and require significantly greater IM resolving power to separate than is commercially available. While MD simulations of other CDSA reaction products postulate that bulkier counterions, like triflate or hexafluorophosphate, can bind to the central void of larger supramolecular complexes and coordinate to metal centers [27], our results suggest that when nitrate is present, it is tightly bound to one of the Pt coordination sites.

Currently, commercial drift tube–based IM instrumentation (e.g., Agilent 6560 IMS-Q-TOF) is unsuitable for first-principles determination of CCS of fragile complexes due to the post-mobility collision cell which cannot be tuned to preserve intact, high-charge complexes without significantly reducing the resolving power of the mobility separation (data not shown) [30,

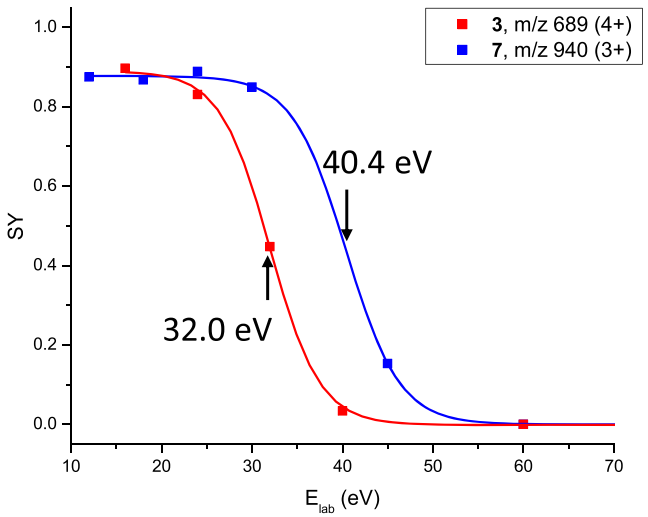

Figure 3. Plots of survival yield (SY) of the CID precursor ions as a function of their laboratory-frame collision energies (E_{lab}). Sigmoidal fits of each SY data set reveal inflection points corresponding to the $E_{lab,50}$ of 32.0 eV and 40.4 eV for the nitrate-free rhomboid (**3**, red) and nitrate-adducted rhomboid (**7**, blue) ions, respectively

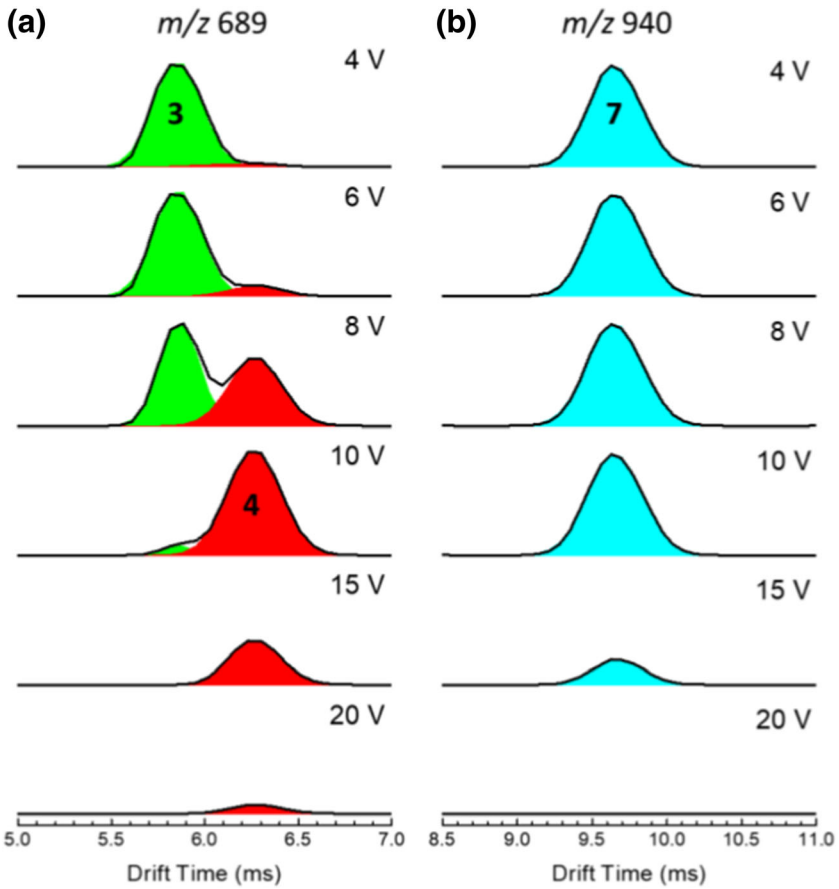

Figure 4. Gaussian peak-fitting IM spectra resulting from CID of the (**a**) isobaric nitrate-free rhomboid (**3**, 5.86 ms, green) and half-rhomboid (**4**, 6.25 ms, red) and (**b**) the nitrate-adducted rhomboid (**7**, 9.67 ms, blue)

31]. Reduction of the potentials of the post-IM collision cell leads to the largest reduction of ion heating effects allowing for transmission and mass detection of fragile complexes; however, reduction of these potentials slows the ions, which leads to diffusional broadening of the observed IM spectra such that any CCS information is lost. Additionally, the potential for post-IM fragmentation severely complicates assignment of IM signals for CCS determination as ions will transmit through the drift tube as high-order complexes but be identified as fragments or dissociation products. Thus, for first-principles determination of CCS of fragile CDSA reaction product complexes, home-built or modified commercial instrumentation must be used [27].

Overall, we observe that careful instrument tuning is required to observe intact, anion-free CDSA reaction products in high relative abundances. CID provides topological confirmation of the expected reaction products and suggests that when observed, nitrate adducts are specifically coordinated to Pt centers. Nitrate adducts mitigate effects of Coulombic repulsion in the gas phase as the nitrate-adducted reaction products survive at higher collision energies than the nitrate-free analogue. The gas-phase observations made herein may suggest that in the condensed phase, charge neutralization with counterions may improve the stability of larger reaction products, like 3D geometries or sheet-like reaction products [7], and that these effects may be beyond attractive Coulombic effects (*viz.* negatively charged counterions binding non-specifically to positively charged reaction products). While anionic adducts are often ignored (or omitted) when reporting MS or IM-MS results of supramolecular complexes, the comparative effects of other anions (e.g., triflate, hexafluorophosphate) may prove valuable to the design of larger CDSA products where Coulombic repulsion effects may prevent observation of intact products either by condensed-phase or gas-phase characterization techniques. The rational design of the shape and structure of CDSA reaction products can be tested by CID with results correlated to condensed-phase chemistries and to specific effects of adduction of other anionic counterions. While the effects observed herein are limited to the gas phase, condensed-phase reaction products will likely bind anions resulting from Coulombic attraction, which may affect the stability or intended performance of reaction products. Overall, gas-phase characterization of CDSA ions must be performed below their respective dissociation thresholds, and CID of intact ions reveals that charge reduction through adduction of anions results in increased stability of lower charged reaction products in the gas phase.

Conclusion

Detection and characterization of fragile complexes by MS and IM-MS must be performed carefully to minimize effects of

collisional activation. By carefully tuning IM-MS instruments for small molecules and complexes in a similar protocol to what has been published for proteins, large, intact reaction products have been observed from solution mixtures of reaction precursors. When MS signals overlap, the IM peak areas can be used for determination of relative abundance of isobaric ions. An additional benefit of determining relative abundance for CID experiments using extracted IM spectra includes the ability to focus on pre-mobility dissociation rather than the ensemble of all post mass selection dissociation events as pre-mobility dissociation will result in product ions with unique drift times; whereas, post-mobility fragmentation will result in *m/z* of the dissociation product ions but with the drift time (or arrival time) of the precursor ions.

The IM-MS data clearly show singular, gas-phase conformations and structures for the precursor and product ions of CID as each identified ion can be fit to singular Gaussian peaks, supporting the notion that these ions are rigid in structure and conformationally homogeneous. The results of CID reveal the fragmentation pathways, and neutral and charged dissociation products help to confirm the topology of the mass-selected reaction product ions and identify coordination sites of anionic adducts. Additionally, the SY results provide a basis for comparison of the stability of reaction products. They show that the gas-phase stability of these supramolecular complex ions is dependent on the supramolecular or macromolecular shape and charge rather than the number of Pt–N bonds. Application of IM-MS to the characterization of small molecules and labile complexes requires careful tuning to preserve solution-phase structures. IM-MS provides structural characterization of supramolecular complexes which may not be achieved by traditional spectroscopic techniques and serves as a potential high-throughput approach for characterizing CDSA reaction products once instrument tuning is complete.

References

1. Whitesides, G.M., Grzybowski, B.: Self-assembly at all scales. Science. **295**(5564), 2418–2421 (2002)
2. Northrop, B.H., Zheng, Y.R., Chi, K.W., Stang, P.J.: Self-organization in coordination-driven self-assembly. Acc. Chem. Res. **42**(10), 1554–1563 (2009)
3. Baxter, P.N.W., Lehn, J.M., Baum, G., Fenske, D.: The design and generation of inorganic cylindrical cage architectures by metal-ion-directed multicomponent self-assembly. Chem. Eur. J. **5**(1), 102–112 (1999)
4. Lehn, J.M., Rigault, A., Siegel, J., Harrowfield, J., Chevrier, B., Moras, D.: Spontaneous assembly of double-stranded helicates from oligobipyridine ligands and copper(I) cations - structure of an inorganic double helix. Proc. Natl. Acad. Sci. U. S. A. **84**(9), 2565–2569 (1987)
5. Kramer, R., Lehn, J.M., Marquis-Rigault, A.: Self-recognition in helicate self-assembly - spontaneous formation of helical metal-complexes from mixtures of ligands and metal-ions. Proc. Natl. Acad. Sci. U. S. A. **90**(12), 5394–5398 (1993)
6. Stang, P.J., Olenyuk, B.: Self-assembly, symmetry, and molecular architecture: coordination as the motif in the rational design of supramolecular metallacyclic polygons and polyhedra. Acc. Chem. Res. **30**(12), 502–518 (1997)
7. Datta, S., Saha, M.L., Stang, P.J.: Hierarchical assemblies of supramolecular coordination complexes. Acc. Chem. Res. **51**(9), 2047–2063 (2018)
8. Zhou, Z., Yan, X., Cook, T.R., Saha, M.L., Stang, P.J.: Engineering functionalization in a supramolecular polymer: hierarchical self-organization of triply orthogonal non-covalent interactions on a supramolecular coordination complex platform. J. Am. Chem. Soc. **138**(3), 806–809 (2016)
9. Saha, M.L., Yan, X., Stang, P.J.: Photophysical properties of organoplatinum(II) compounds and derived self-assembled metallacycles and metallacages: fluorescence and its applications. Acc. Chem. Res. **49**(11), 2527–2539 (2016)
10. Fujita, D., Ueda, Y., Sato, S., Mizuno, N., Kumasaka, T., Fujita, M.: Self-assembly of tetravalent Goldberg polyhedra from 144 small components. Nature. **540**(7634), 563 (2016)
11. Hoshino, M., Khutia, A., Xing, H., Inokuma, Y., Fujita, M.: The crystalline sponge method updated. IUCrJ. **3**(Pt 2), 139–151 (2016)
12. Yoneya, M., Tsuzuki, S., Yamaguchi, T., Sato, S., Fujita, M.: Coordination-directed self-assembly of M12L24 nanocage: effects of kinetic trapping on the assembly process. ACS Nano. **8**(2), 1290–1296 (2014)
13. Chan, Y.T., Li, X., Soler, M., Wang, J.L., Wesdemiotis, C., Newkome, G.R.: Self-assembly and traveling wave ion mobility mass spectrometry analysis of hexacadmium macrocycles. J. Am. Chem. Soc. **131**(45), 16395–16397 (2009)
14. Chan, Y.T., Li, X., Yu, J., Carri, G.A., Moorefield, C.N., Newkome, G.R., Wesdemiotis, C.: Design, synthesis, and traveling wave ion mobility mass spectrometry characterization of iron(II)- and ruthenium(II)-terpyridine metallomacrocycles. J. Am. Chem. Soc. **133**(31), 11967–11976 (2011)
15. Li, X., Chan, Y.T., Newkome, G.R., Wesdemiotis, C.: Gradient tandem mass spectrometry interfaced with ion mobility separation for the characterization of supramolecular architectures. Anal. Chem. **83**(4), 1284–1290 (2011)
16. Cook, T.R., Zheng, Y.R., Stang, P.J.: Metal-organic frameworks and self-assembled supramolecular coordination complexes: comparing and contrasting the design, synthesis, and functionality of metal-organic materials. Chem. Rev. **113**(1), 734–777 (2013)
17. Cook, T.R., Stang, P.J.: Recent developments in the preparation and chemistry of metallacycles and metallacages via coordination. Chem. Rev. **115**(15), 7001–7045 (2015)
18. Yam, V.W., Au, V.K., Leung, S.Y.: Light-emitting self-assembled materials based on d(8) and d(10) transition metal complexes. Chem. Rev. **115**(15), 7589–7728 (2015)
19. Hong, C.M., Bergman, R.G., Raymond, K.N., Toste, F.D.: Self-assembled tetrahedral hosts as supramolecular catalysts. Acc. Chem. Res. **51**(10), 2447–2455 (2018)
20. Zhang, D., Ronson, T.K., Nitschke, J.R.: Functional capsules via subcomponent self-assembly. Acc. Chem. Res. **51**(10), 2423–2436 (2018)
21. Jurneczko, E., Barran, P.E.: How useful is ion mobility mass spectrometry for structural biology? The relationship between protein crystal structures and their collision cross sections in the gas phase. Analyst. **136**(1), 20–28 (2011)
22. Bohrer, B.C., Merenbloom, S.I., Koeniger, S.L., Hilderbrand, A.E., Clemmer, D.E.: Biomolecule analysis by ion mobility spectrometry. Annu Rev Anal Chem (Palo Alto, Calif). **1**(1), 293–327 (2008)
23. Bleiholder, C., Bowers, M.T.: The solution assembly of biological molecules using ion mobility methods: from amino acids to amyloid beta-protein. Annu Rev Anal Chem (Palo Alto, Calif). **10**(1), 365–386 (2017)
24. Kind, T., Fiehn, O.: Seven Golden Rules for heuristic filtering of molecular formulas obtained by accurate mass spectrometry. BMC Bioinf. **8**, 105 (2007)
25. Shi, L., Holliday, A.E., Glover, M.S., Ewing, M.A., Russell, D.H., Clemmer, D.E.: Ion mobility-mass spectrometry reveals the energetics of intermediates that guide polyproline folding. J. Am. Soc. Mass Spectrom. **27**(1), 22–30 (2016)
26. Gaye, M.M., Nagy, G., Clemmer, D.E., Pohl, N.L.: Multidimensional analysis of 16 glucose isomers by ion mobility spectrometry. Anal. Chem. **88**(4), 2335–2344 (2016)
27. Brocker, E.R., Anderson, S.E., Northrop, B.H., Stang, P.J., Bowers, M.T.: Structures of metallosupramolecular coordination assemblies can be obtained by ion mobility spectrometry-mass spectrometry. J. Am. Chem. Soc. **132**(38), 13486–13494 (2010)

28. Chen, S.H., Russell, D.H.: How closely related are conformations of protein ions sampled by IM-MS to native solution structures? J. Am. Soc. Mass Spectrom. **26**(9), 1433–1443 (2015)
29. Morsa, D., Gabelica, V., De Pauw, E.: Effective temperature of ions in traveling wave ion mobility spectrometry. Anal. Chem. **83**(14), 5775–5782 (2011)
30. Harrison, J. A.; Kelso, C.; Pukala, T. L.; Beck, J. L.: Conditions for analysis of native protein structures using uniform field drift tube ion mobility mass spectrometry and characterization of stable calibrants for TWIM-MS. J. Am. Soc. Mass. Spectrom. **30**(2), 256-267(2019)
31. Gabelica, V., Livet, S., Rosu, F.: Optimizing native ion mobility Q-TOF in helium and nitrogen for very fragile noncovalent structures. J. Am. Soc. Mass Spectrom. **29**(11), 2189–2198 (2018)
32. Giles, K., Williams, J.P., Campuzano, I.: Enhancements in travelling wave ion mobility resolution. Rapid Commun. Mass Spectrom. **25**(11), 1559–1566 (2011)
33. Ruotolo, B.T., Benesch, J.L., Sandercock, A.M., Hyung, S.J., Robinson, C.V.: Ion mobility-mass spectrometry analysis of large protein complexes. Nat. Protoc. **3**(7), 1139–1152 (2008)
34. Duez, Q., Chirot, F., Lienard, R., Josse, T., Choi, C., Coulembier, O., Dugourd, P., Cornil, J., Gerbaux, P., De Winter, J.: Polymers for traveling wave ion mobility spectrometry calibration. J. Am. Soc. Mass Spectrom. **28**(11), 2483–2491 (2017)
35. Haler, J.R.N., Kune, C., Massonnet, P., Comby-Zerbino, C., Jordens, J., Honing, M., Mengerink, Y., Far, J., De Pauw, E.: Comprehensive ion mobility calibration: poly(ethylene oxide) polymer calibrants and general strategies. Anal. Chem. **89**(22), 12076–12086 (2017)
36. Patiny, L., Borel, A.: ChemCalc: a building block for tomorrow's chemical infrastructure. J. Chem. Inf. Model. **53**(5), 1223–1228 (2013)
37. Kune, C., Far, J., De Pauw, E.: Accurate drift time determination by traveling wave ion mobility spectrometry: the concept of the diffusion calibration. Anal. Chem. **88**(23), 11639–11646 (2016)
38. Bush, M.F., Campuzano, I.D.G., Robinson, C.V.: Ion mobility mass spectrometry of peptide ions: effects of drift gas and calibration strategies. Anal. Chem. **84**(16), 7124–7130 (2012)
39. Smith, D.P., Knapman, T.W., Campuzano, I., Malham, R.W., Berryman, J.T., Radford, S.E., Ashcroft, A.E.: Deciphering drift time measurements from travelling wave ion mobility spectrometry-mass spectrometry studies. Eur. J. Mass Spectrom. (Chichester). **15**(2), 113–130 (2009)